Cell Reports
Article

Cell-Cycle-Dependent Reconfiguration of the DNA Methylome during Terminal Differentiation of Human B Cells into Plasma Cells

Gersende Caron,[1,2,3,4] Mourad Hussein,[1,3,4] Marta Kulis,[5] Céline Delaloy,[1,3,4] Fabrice Chatonnet,[1,2,3,4] Amandine Pignarre,[1,3,4] Stéphane Avner,[3,6] Maud Lemarié,[1,3,4] Elise A. Mahé,[3,6] Núria Verdaguer-Dot,[5] Ana C. Queirós,[5] Karin Tarte,[1,2,3,4] José I. Martín-Subero,[5] Gilles Salbert,[3,6,*] and Thierry Fest[1,2,3,4,*]
[1]INSERM, UMR917, Equipe labellisée Ligue contre le Cancer, Rennes 35043, France
[2]Pôle de Biologie, Centre Hospitalier Universitaire (CHU), Rennes 35033, France
[3]Université de Rennes 1, Rennes 35065, France
[4]Etablissement Français du Sang de Bretagne, Rennes 35016, France
[5]Departamento de Anatomía Patológica, Farmacología y Microbiología, Universitat de Barcelona, Institut d'Investigacions Biomèdiques August Pi i Sunyer (IDIBAPS), 08036 Barcelona, Spain
[6]Centre national de la recherche scientifique (CNRS), UMR6290, Rennes 35042, France
*Correspondence: gilles.salbert@univ-rennes1.fr (G.S.), thierry.fest@univ-rennes1.fr (T.F.)
http://dx.doi.org/10.1016/j.celrep.2015.09.051

SUMMARY

Molecular mechanisms underlying terminal differentiation of B cells into plasma cells are major determinants of adaptive immunity but remain only partially understood. Here we present the transcriptional and epigenomic landscapes of cell subsets arising from activation of human naive B cells and differentiation into plasmablasts. Cell proliferation of activated B cells was linked to a slight decrease in DNA methylation levels, but followed by a committal step in which an S phase-synchronized differentiation switch was associated with an extensive DNA demethylation and local acquisition of 5-hydroxymethylcytosine at enhancers and genes related to plasma cell identity. Downregulation of both TGF-β1/SMAD3 signaling and p53 pathway supported this final step, allowing the emergence of a CD23-negative subpopulation in transition from B cells to plasma cells. Remarkably, hydroxymethylation of *PRDM1*, a gene essential for plasma cell fate, was coupled to progression in S phase, revealing an intricate connection among cell cycle, DNA (hydroxy) methylation, and cell fate determination.

INTRODUCTION

Production of antibody-secreting cells from B cells is crucial for adaptive immunity and involves a number of mechanisms controlling B cell differentiation into plasmablast. B cell fate determination proceeds autonomously and stochastically (Duffy et al., 2012; Tangye et al., 2003) from a balance between division and death, both parameters remaining highly variable at the single-cell level (Duffy et al., 2012).

Control of terminal B cell differentiation by transcription factors operates following specific timing and pace that remain only partially understood. A large number of external and internal signals and cues impact this process by influencing transcriptional cascades (Allman and Cancro, 2011). BCL6 has an antagonistic role to the plasmablast fate-determining transcription factor BLIMP1, encoded by *PRDM1*, in lineage determination. These two factors mutually inhibit each other, BLIMP1 having a broad role in promoting plasma cell (PC) differentiation through the repression of B cell signature genes including *c-Myc*, *CIITA*, *SPIB*, *LMO2*, and *PAX5* (Cubedo et al., 2011; Martins and Calame, 2008). BLIMP1 acts as a sequence-specific recruitment factor for chromatin-modifying enzymes and corepressors (Martins and Calame, 2008), and, even though earliest stages of plasmablast commitment do not seem to require BLIMP1 (Kallies et al., 2004), high BLIMP1 expression levels matter for maturation and maintenance of long-lived PCs (Kallies et al., 2007). Both IRF4 and XBP-1 also are required for PC differentiation. If the latter acts downstream of BLIMP1, it is still unclear how IRF4 is positioned (Nutt et al., 2011). In human centrocytes, IRF4 is expressed concomitantly with BLIMP1 (Cattoretti et al., 2006), and in mouse, secreted IgM is detected in the absence of functional BLIMP1, suggesting the existence of a preplasmablast state (Kallies et al., 2007; Kuo et al., 2007) that could be represented in human by B cells expressing low levels of *PAX5* and *PRDM1* associated to high *IRF4* levels (Jourdan et al., 2011). Finally, the existence of critical thresholds for specific transcription factors (Kallies et al., 2004; Ochiai et al., 2013) suggests the establishment of multilayered repression loops between these factors, a process driving B cell fate in an autonomous and stochastic manner and most likely coordinated at an epigenetic level.

Hematopoiesis involves reprogramming of epigenetic modifications associated with development (Cedar and Bergman, 2011). Cell cycle, and in particular DNA synthesis during S phase, provides a window of opportunity for chromatin remodeling of genes from an inactive to an active state during

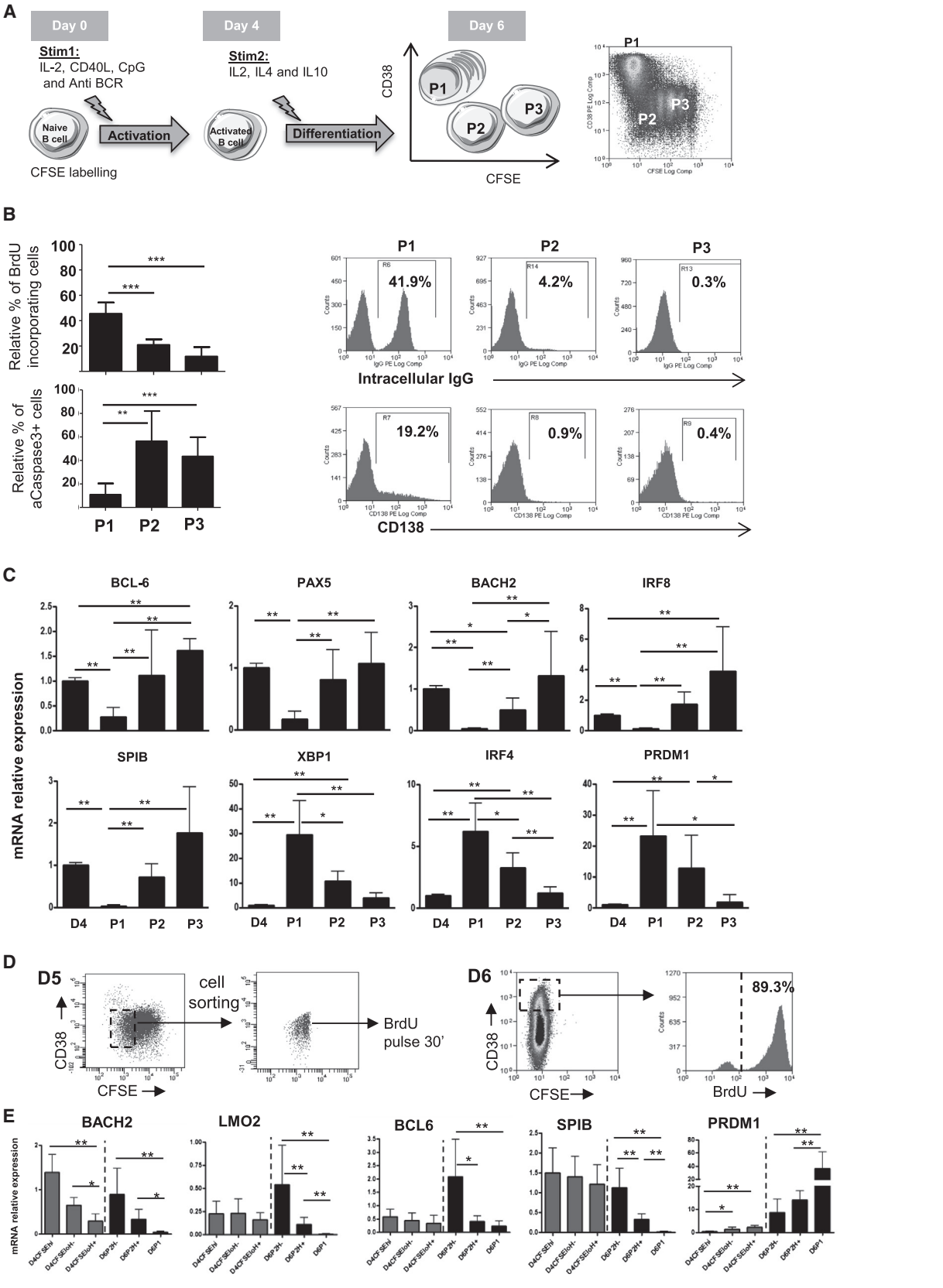

(legend on next page)

hematopoietic cell differentiation (Bird, 2002; Bird et al., 1998; Pop et al., 2010). For instance, during CD4+ helper T cell differentiation, intricate proliferation and differentiation signals lead to erasure of epigenetic constraints, such as DNA methylation at CpGs (Bird et al., 1998). DNA methylation may directly interfere with the binding of transcription factors to their cognate DNA sequences or may enable recruitment of methyl-CpG-binding proteins, which induce a repressed chromatin environment (Bird, 2002). Kriaucionis and Heintz (2009) showed the presence of 5-hydroxymethylcytosine (5hmC) in brain DNA and suggested that this DNA state could represent an oxidative intermediate in a pathway of active DNA demethylation with potentially important biological roles. Accordingly, 5hmC was later found to be enriched at active genes and enhancers, as well as at the start sites of genes whose promoters bear dual H3K27me3 and H3K4me3 marks (Mellén et al., 2012; Pastor et al., 2011; Sérandour et al., 2012; Stroud et al., 2011). Simultaneously, the production of 5hmC through hydroxylation of the methyl group of 5-methylcytosine by TET1 protein was demonstrated in mammalian cells (Tahiliani et al., 2009). The discovery that TET proteins are involved in self-renewal of stem cells, cell differentiation, and reprogramming opened new perspectives for the understanding of cell plasticity (Koh et al., 2011; Madzo et al., 2014; Szulwach et al., 2011).

Here by activating human naive B cells (NBCs) in vitro (Le Gallou et al., 2012), we captured heterogeneous B cell fates and early committed states otherwise too transient to be identified by in vivo analyses. Cells undergoing exponential growth upon stimulation were sorted and subsequently analyzed, allowing the identification of multiple cell subsets based on lineage-specific gene expression. Our results show an entanglement between cell division and differentiation programs along with a cellular machinery largely open toward apoptosis. The final step of commitment, when a human B cell ended as a plasmablast, was captured and found to be synchronized with the cell cycle and associated with a dynamic demethylation process involving 5hmC apposition on plasmablast fate-determining genes.

RESULTS

Cell Proliferation Sustains Plasmablast Generation

Carboxyfluoroescein diacetate succinimidyl ester (CFSE)-labeled human CD19+CD27− NBCs were differentiated in vitro as described in Figure 1A (Le Gallou et al., 2012). We have shown previously that the first days of the culture are associated with a transcriptional burst and proliferation in response to the activation cocktail. At day 4 (D4), cells presented a downregulation of *BCL-6*, *BACH2*, and *PAX5* and started to upregulate *PRDM1*, *XBP1*, and *IRF4* compared to NBCs. These modifications were more pronounced in CFSElow compared to CFSEhigh cells, which is consistent with a commitment to the plasmablast fate linked to high proliferation.

We next focused on the process of terminal differentiation. At D6, CD38 and CFSE detection allowed discrimination of three cell populations, hereafter referred to as P1, P2, and P3 (Figure 1A). BrdU uptake, active caspase-3 and CD138 membrane expression, as well as intracellular IgG staining showed that P1 cells corresponded to proliferative plasmablasts able to undergo class switch recombination and to give rise to CD138+ PCs (Figure 1B). Both P2 and P3 corresponded to highly apoptotic post-activated B cells containing a low fraction of cycling cells, in which both cell death and low proliferation could be counterbalanced by CD40L/NF-κB pathway activation (data not shown), suggesting that apoptosis observed in those cells mainly was due to the removal of the activation cocktail rather than a vital exhaustion that could be expected after a 6-day culture. Expression of eight selected genes (Figure 1C) confirmed that P1 corresponded to plasmablasts characterized by elevated *XBP1*, *PRDM1*, and *IRF4* and decreased *SPIB*, *BCL-6*, *PAX5*, *BACH2*, and *IRF8* mRNA levels. Interestingly, compared to D4 and unlike P3, P2 cells upregulated *PRDM1*, *IRF4*, and *XBP1*, whereas *BCL-6* and *PAX5* presented nonsignificant changes, suggesting that P2 forms a heterogeneous compartment containing cells committed to plasmablastic fate. The proportion of cycling P2 cells was quite stable throughout experiments (≈20%, n = 8) and not affected when apoptosis was inhibited (data not shown). We next sorted out the P2 compartment at D5 and labeled it for 30' with BrdU before putting cells back in culture for 24 hr. At D6, emerging P1 cells were 90.4% ± 3.8% (n = 3) positive for BrdU (Figure 1D), indicating that dividing P2 cells contain plasmablasts precursors. Conversely, sorted P3 cells were unable to generate P1 cells (data not shown).

To analyze gene expression profiles of cells engaged in cell division (i.e., >2N DNA content) compared to those in G0/G1, cells were stained with Hoechst before sorting several cell subsets at D4 and D6. As early as D4 among the five selected genes, a significant downregulation of *BACH2* was found in Hoechst-positive (S and G2/M phases) compared to Hoechst-negative (G1 phase) cells, reflecting an early commitment of the former cells toward plasmablasts (Figure 1E). At D6, cycling P2 cells

Figure 1. Relationship between Cell Proliferation and B Cell Fate

(A) CFSE-labeled NBCs were differentiated using a two-step cell culture process giving rise to three different cell populations called P1, P2, and P3, according to CFSE dilution and CD38 expression at D6.

(B) Proliferation and apoptosis of the three generated populations at D6 were determined, respectively, using BrdU incorporation and active caspase-3 staining (percentage of positive cells ± SD; n = 8). Intracellular IgG and membrane expression of CD138 also were evaluated at D6 by FACS analysis (one representative experiment among five).

(C) Transcriptional profiling of eight genes was done using qRT-PCR on sorted P1, P2, P3, and D4 cells. Results are expressed relative to gene expression in B cells at D4 (mean values ± SD; n = 5).

(D) P2 compartment was sorted out at D5, labeled for 30 min with BrdU, and analyzed at D6 for CD38 expression and BrdU labeling (one representative experiment among four).

(E) Cells were sorted at D4 in CFSEhigh and CFSElow cycling (Hoechst+, H+) or not (Hoechst−, H−) and at D6 in P1, P2 cycling (H+), or not (H−). Transcriptional analysis was performed by qRT-PCR and results are expressed relative to gene expression in a pool of tonsil B cells (mean values ± SD; n = 5; $^{*}p < 0.05$, $^{**}p < 0.01$, $^{***}p < 0.001$).

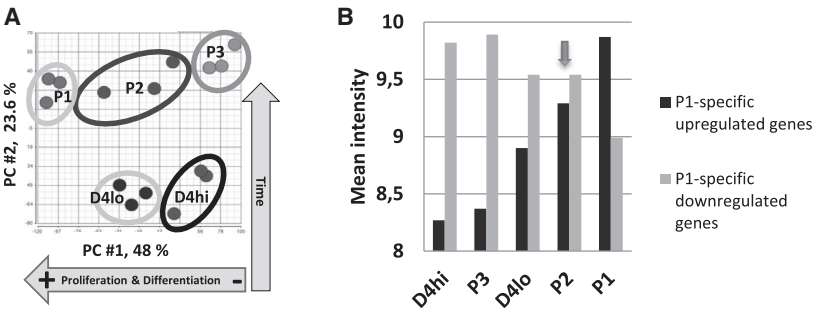

C

Comparison	TOP-5 Molecular & Cellular Function	Top-5 Upstream Regulator, Prediction* (*p*-value of overlap)
P1 *vs.* P2	**Cell death & survival (5.48^{-11}- 2.64^{-2})**	**TP53, I** (4.39^{-11})
	Cellular development	CD40, NSp (1.20^{-8})
	Cell growth & proliferation	E2F4 , NSp(1.24^{-8})
	Cell cycle	IFNG, I (3.92^{-7})
	Cellular assembly & organization	NUPR1, I (4.87^{-7})
P1 *vs.* D4lo	**Cell death & survival (7.43^{-10}- 2.51^{-2})**	IFNG, I (6.47^{-9})
	Cellular development	CSF2 , I (1.05^{-8})
	Gellular growth & proliferation	IL1RN, A (1.60^{-8})
	Post-translation modification	IFNA2 , I (9.17^{-8})
	Protein folding	**TP53, NSp** (3.12^{-7})
D4lo *vs.* D4hi	Post-translation modification	**TP53, I** (5.9^{-12})
	Protein folding	E2F4 , NSp (2.7^{-8})
	Cell Cycle	E2F1 , NSp (2.7^{-7})
	Cell death & survival (7.68^{-5}- 4.92^{-2})	Mek , A (1.9^{-6})
	Cellular development	RB1 , NSp (4.7^{-5})

Figure 2. Cell Type-Specific Gene Expression in P1, P2, and P3 Generated Populations

(A) The one-way repeated-measures ANOVA with an FDR < 5% was used on the raw data, allowing us to generate 9,599 probe sets corresponding to 5,632 single genes. The principal component analysis revealed for the first (PC1, with 48% of the variables) and second (PC2, with 23.6% of the variables) components a specific ordering among cell populations following a proliferation and differentiation axis.

(B) Unsupervised hierarchical clustering allowed defining P1-specific up- and downregulation signatures including 1,794 genes and 2,534 genes, respectively. We compared the log2 mean intensity of each signature for all cell populations. The arrow indicates the specific position for P2 cells.

(C) Top 5 molecular and cellular functions and top 5 upstream regulators was obtained using Ingenuity software analysis. The asterisk relates to the prediction abbreviations (A, activated; I, inactivated; NSp, not specified; NE, not evaluated because excluded from the dataset; NS, not significant).

completed their commitment with the downregulation of *LMO2*, *BCL-6*, and *SPIB*, leading to a gene expression pattern close to P1 cells. These results indicate the need for further cell divisions beyond D4 to complete plasmablastic differentiation. In contrast, the upregulation of *LMO2* and *BCL6* expression in the Hoechst-negative P2 subset indicated that these cells drifted away from a PC destiny (Figure 1E).

Concomitant p53 Pathway Inhibition and G1/S Transition Promotion in P1 Committed Cells

To determine the transcriptional program sustaining plasmablast emergence, we performed microarray-based gene expression profiling comparing five paired cell subsets, including CFSElow and CFSEhigh cells obtained at D4 (hereafter referred as D4lo and D4hi) and P1, P2, and P3 sorted at D6 (Figure S1A). Principal component analysis allowed drawing a common proliferation and differentiation axis along which P2 cells occupied an intermediate position between the most and less polarized P1 and P3 cells, respectively (Figure 2A). Unsupervised clustering showed that P1 cells were hierarchically separated from the others and were characterized by 1,794 P1-specific upregulated genes and 2,534 P1-specific downregulated genes (Figure S1B). By computing the mean log2 intensity for both gene lists on each cell population, we confirmed the proliferation-based hierarchical cell classification with P2 being at a crossroad position, suggesting that in our model these cells can either progress to P1 or to cell death (Figure 2B).

We next established gene lists of factors differentially expressed between P1 and P2, P1 and D4lo, as well as D4lo and D4hi. By using Ingenuity software, we found that the most prominent function that differed in P1 versus P2 was cell death and survival, and the top 5 upstream regulators predicted inactivation of the p53 pathway in P1 with the highest significance (Figure 2C). Although dead cells were removed from this transcriptomic analysis, we could not exclude an impact of the presence of potentially apoptotic P2 cells. However, the observations made by comparing P2 and P1 cells were already apparent in D4lo compared to D4hi, two populations that are not apoptotic (data not shown). The p53 pathway analysis revealed that 32 of 79 genes (40%) related to this pathway had a differential expression in P1 compared to P2, of which 19 varied significantly ($p < 0.05$) (listed in Table S1). Although *TP53* expression itself was not significantly modified in P1 cells in microarray data, qRT-PCR analysis showed a consistent downregulation (Figure S1C). Inactivation of the p53 pathway was evidenced by upregulation of *MDM2* as well as *BCL2L1* and *BIRC5*—two genes inhibited by p53—while *NOXA*, a p53-activated gene, was downregulated. As expected for PC precursors, *BCL2* showed a striking downregulation in P1 cells, counterbalanced by an upregulation of *BCL2L1*. Overall, the P1 population was characterized by a decreased susceptibility to cell death and an inactivation of the p53 pathway, which should allow for a potent induction of G1/S phase transition as well as progression in S phase (Yin et al., 1992; Zhang et al., 2000). Pathway analysis identified a G1/S transition promotion in P1 cells, characterized by a pronounced downregulation of the TGF-β1/SMAD3 pathway associated with an increased expression of *CDC25A* and a promotion of its activity (Ray et al., 2005; Figure S2).

The Last Commitment Step toward Plasmablasts Is Synchronized with the S Phase of the Cell Cycle

To identify P1 founder cells, we looked for differentially expressed cell membrane markers between P1 and P2. In this

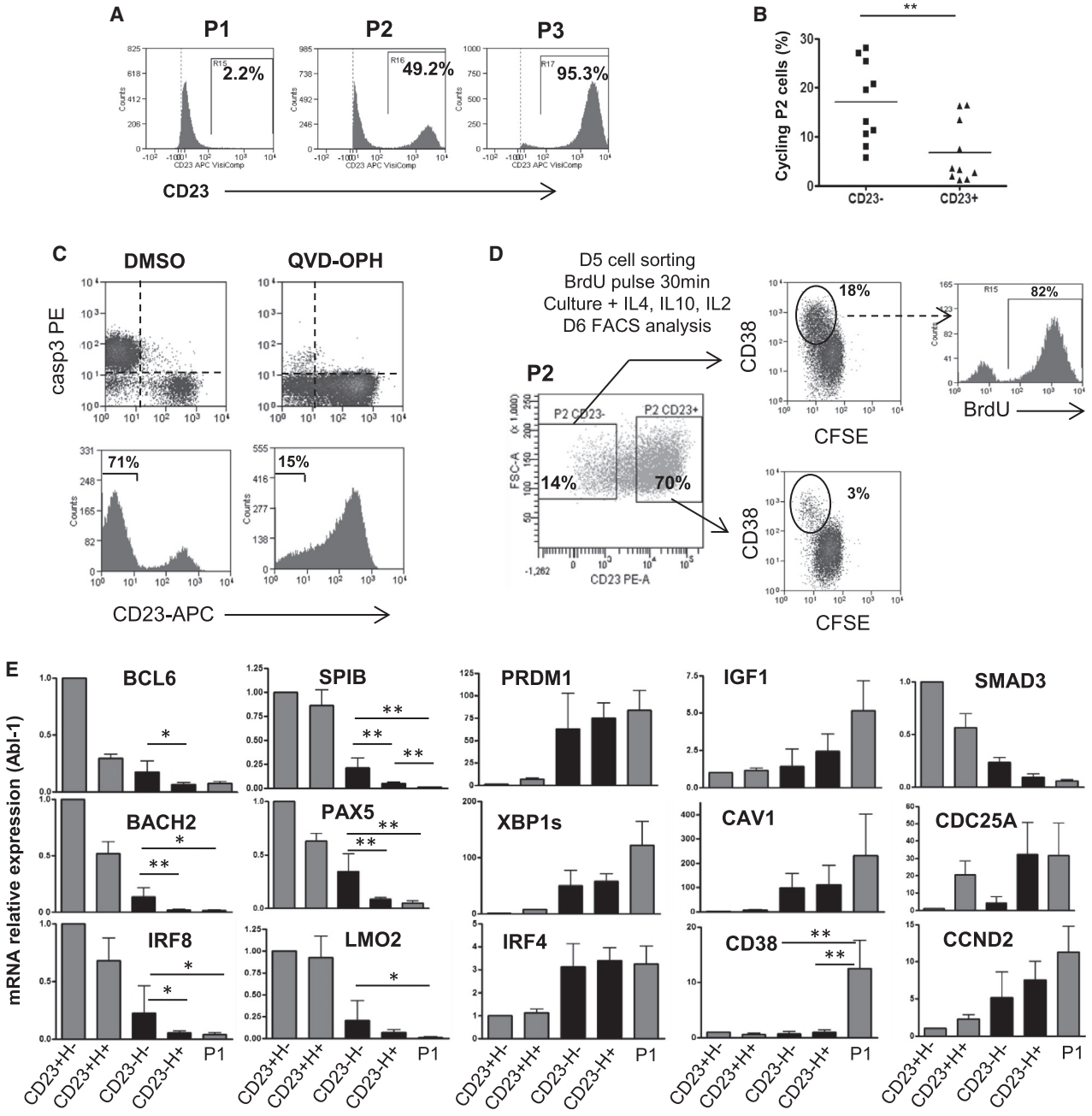

Figure 3. Cycling CD23-Negative P2 Cells Incorporate P1 Founder Cells

(A) FACS analysis of CD23 expression at D6 on P1, P2, and P3 cells. Histogram plots are representative of ten experiments.

(B) Percentage of cycling cells in ten different experiments was evaluated in CD23−/P2 and CD23+/P2 subsets at D6 after Hoechst staining.

(C) Evaluation of apoptosis by active caspase-3 intracellular staining in association with CD23 cell surface staining of P2 cells cultured in the presence of the pan-caspase inhibitor QVD-OPH or DMSO. Dot and histogram plots are representative of four experiments.

(D) CD23− and CD23+ P2 cells cultured in the presence of QVD-OPH were sorted at D5 according to CD23 expression, labeled for 30 min with BrdU, and analyzed at D6 for CD38 expression and BrdU labeling (one representative experiment among four).

(E) Transcriptional analysis of P2 subsets compared to P1 population at D6. CD23+ (gray bars) and CD23− (black bars) P2 cells were divided into cycling (H+) and non-cycling (H−) subsets after a combined CD23/Hoechst staining and cell sorting. Results are expressed relative to gene expression in CD23+/H−/P2 cells (mean values ± SD; n = 5). Only statistics between CD23− subsets and P1 cells are represented (*p < 0.05; **p < 0.01).

context, we evidenced an inhibition of the IL-4 pathway in P1, secondary to *STAT6* downregulation and associated with decreased expression of *IL4R*, *CD23*, and *CIITA* targets (Figure S3A). Consistent with this finding, expression of CD23 at the cell surface was negative for P1, positive for P3, and bimodal for P2 (Figure 3A). Flow cytometry analysis of cytokine-deprived

D6 cells stimulated with IL-4 for 10 min uncovered a striking correlation between intracellular p-STAT6 and membrane CD23 expression, with P1 cells being totally negative for both proteins (Figure S3B). At D6, the number of cycling CD23−/P2 cells was twice that of CD23+ cells (Figure 3B), and, as P1 cells, these cells downregulated membrane IgD, CD83, and HLA-DR expression (data not shown). Of note, more than 70% of these cells were caspase-3a+, indicating that dying cells lose the CD23 marker likely through a process different from STAT6 inhibition since the proportion of CD23−/P2 cells fell to 10%–20% in the presence of the pan-caspase inhibitor Q-VD-OPH added at D4 (Figure 3C). Since CD23 could be lost on apoptotic cells, cell sorting of CD23− and CD23+ P2 cells was performed in the presence of Q-VD-OPH in order to capture cells that have downregulated CD23 expression in an apoptotic-independent manner. As expected, CD23− cells presented a higher propensity to give rise to P1, indicating that the non-apoptotic CD23− subset of P2 hosts plasmablastic founder cells (Figure 3D). However, although it does not affect differentiation, the use of Q-VD-OPH is still an artificial way to get rid of apoptotic cells that are losing CD23. In the absence of the pan-caspase inhibitor, caspase-3+ cells were excluded from cell sorting using a permeable detection system for active caspase-3, and, as previously observed, CD23− cells presented a better capacity to differentiate than the CD23+/P2 cells (Figure S4A). Finally, BrdU pulse-chase experiments confirmed that plasmablasts emerged from cycling CD23−/P2 cells (Figure 3D).

We next sorted out subsets of Hoechst-positive (H+) and -negative cells (H−) at D6 from the CD38low/CD23−/CFSElow compartment (for gating strategy, see Figure S3C, top), and we performed qRT-PCR analysis on genes selected based on microarray data in order to determine the potential commitment of these cells to plasmablast differentiation. We evidenced that P2 cells that progress toward P1 fate first downregulate the pSTAT6/CD23 pathway and then, during a unique cell division, end as P1 cells (Figure 3D). Indeed, for almost all tested genes except *CD38*, a shift in the expression patterns between CD23− subsets and CD23+ counterparts was observed (Figure 3E). This result was confirmed even when apoptotic cells were excluded from the analysis (Figure S4B). Likewise, a significant downregulation of B cell identity genes *BCL6*, *BACH2*, *IRF8*, *SPIB*, and *PAX5* was observed in CD23−/H+/P2 cells, with a pattern almost identical to P1 (Figure 3E). This CD23−/H+/P2 subset gained this typical transcriptional profile in cells in S phase, indicating that gene expression changes leading to plasmablasts occurred during an S phase of the cell cycle (Figure S3C).

Plasmablast Commitment Is Associated with a Wide Loss of DNA Methylation

To gain insights into the epigenetic mechanisms modulating gene expression changes observed in our in vitro model, we profiled DNA methylation in different B cell subsets using the Illumina 450K microarray technology. This analysis was done on D0 (NBCs), D4hi, D4lo−/H+, D4lo−/H−, P2/H−, P2/H+, P3, and P1 cell compartments obtained from three different subjects plus tonsil-derived plasmablasts. In unsupervised principal component analysis, NBCs and plasmablasts clustered separately, and the different in-vitro-generated cells were located in between according to a hierarchical ordering. This observation is consistent with previous findings emphasizing the effect of cell proliferation and shows D4lo/H+ and P2/H+ to cluster together at an intermediate position before P1 and plasmablasts purified from tonsils (Figure 4A). These two later showed a marked loss of methylation by unsupervised clustering compared to the other cell populations (Figure 4B). Dot-blot analysis of global 5-methylcytosine (5mC) levels in genomic DNA confirmed the decrease in methylation in P1 cells compared to NBCs (Figure 4C).

We next identified CpGs whose methylation is modulated during terminal B cell differentiation. As compared to NBCs, the CpGs hypomethylated in P1 and purified plasmablasts showed a major overlap (Figure 4D), suggesting that our in vitro model recapitulates the DNA methylation changes that take place in vivo. We then compared DNA methylation patterns of the sequentially obtained cell subpopulations and observed a clear DNA methylation loss between NBCs and D4lo/H+ (4,292 CpGs), which continued in H+/P2 versus D4lo/H+ (518 CpGs) and became particularly extensive in P1 versus H+/P2 (13,660 CpGs) (Figure 4E). Conversely, only very few CpGs became hypermethylated during differentiation (for instance 85 CpGs in P1 versus NBCs). To investigate the functional significance of these epigenetic changes, hypomethylated CpGs were annotated using chromatin state-derived genomic coordinates from immortalized mature B cells (Ernst et al., 2011; Kulis et al., 2012), which showed a DNA methylation profile similar to PCs (Figure 4B). Interestingly, hypomethylated regions showed a specific enrichment in enhancer elements (2.4- to 5-fold, yellow color) as compared to the distribution of the 450K array, in all three comparisons (Figure 4F). This finding suggests that in vitro differentiation of NBCs into plasmablasts associates with a gradual demethylation of enhancers. Furthermore, such demethylation of functional elements frequently targeted genes related to PC differentiation. Indeed, among the 18 selected genes analyzed at the transcriptional level in Figure 3E plus *SDC1* (alias CD138), *CIITA*, and *CCND1*, 13 genes showed a hypomethylation of the 28 CpGs present on the array, when comparing P1 to NBCs (Figure 4G). However, one CpG located within the P1-repressed *SPIB* gene showed a similar behavior, suggesting that hypomethylation, as assessed here, is not necessarily a hallmark of gene activation. In addition, a limitation to these analyses is that the bisulfite treatment used to treat DNA prior to hybridization to the 450K arrays does not discriminate 5mC from 5hmC (Huang et al., 2010), hence limiting the possibility to characterize in detail the molecular mechanisms involved in DNA demethylation during plasmablast commitment.

Molecular and Cellular Functions Involved in Plasmablast Emergence Are Associated with Selective 5hmC Enrichment at PC Identity Genes

To determine if an active DNA demethylation mechanism was involved, genome-wide mapping of 5hmC was undertaken, using a selective chemical labeling (SCL) strategy (Song et al., 2011). Global levels of 5hmC were first analyzed by dot blot and data showed a dramatic decrease in 5hmC during

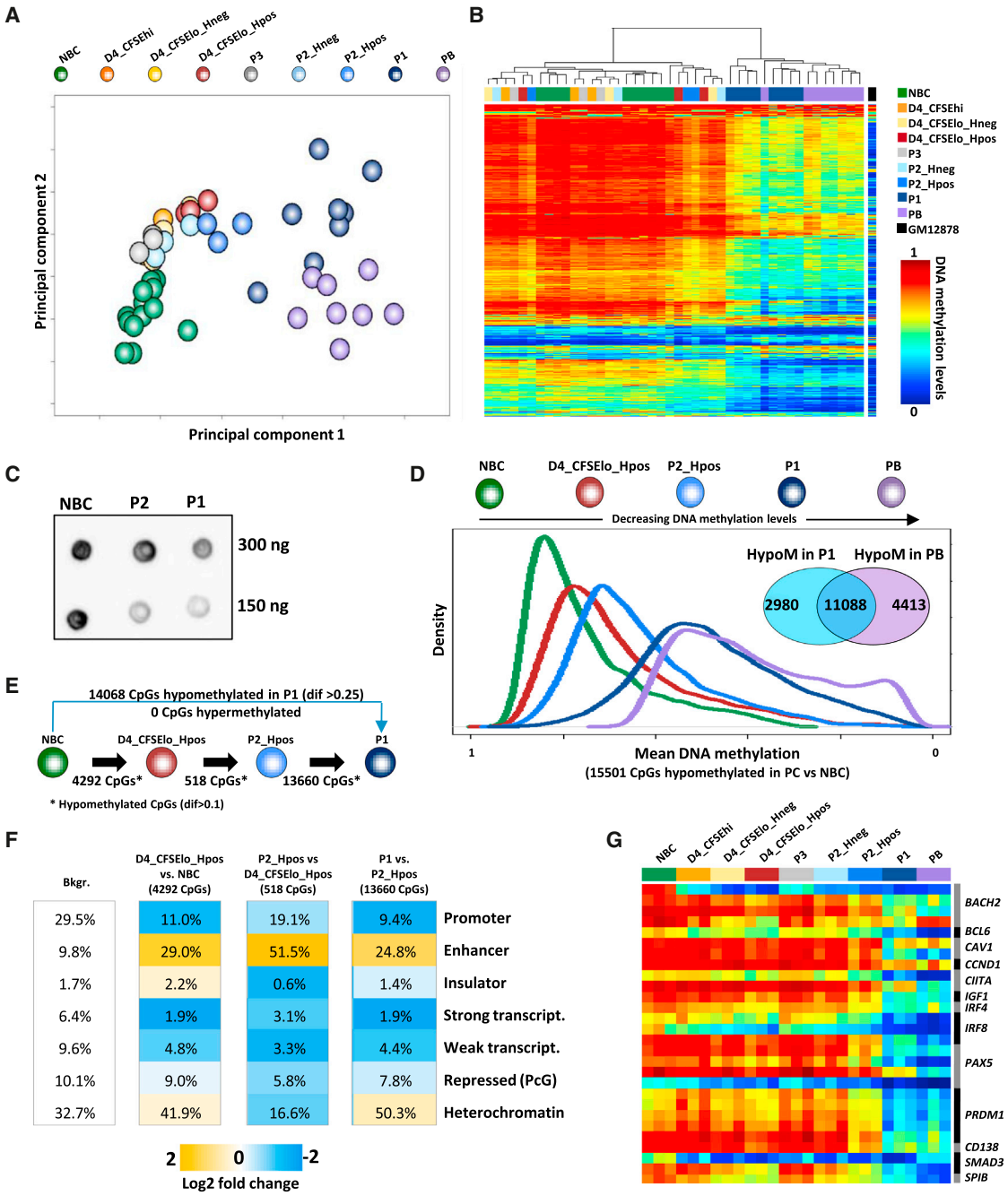

Figure 4. Modulation of the DNA Methylome during In Vitro and In Vivo Differentiation of NBCs into Plasmablasts

(A) Unsupervised principal component analysis of microarray DNA methylation data shows a hierarchical distribution of the samples along an axis going from the less differentiated cells (NBCs, green color at the left) to the most mature tonsil-derived plasmablasts (pink color at the right).

(B) Unsupervised hierarchical clustering of microarray data is shown (28,774 CpGs with SD > 0.1 among of all samples).

(C) The 5mC dot blot shows total genomic DNA from NBCs and D6 P2 and P1 subsets (one representative experiment among three).

(D) Density plot showing the gradual decrease in DNA methylation upon in vitro differentiation of NBCs into P1, which reach a DNA methylation pattern similar to in-vivo-generated plasmablasts. Incrustation: Venn diagram shows the overlap of hypomethylated sites in P1 and plasmablasts as compared to NBCs.

(E) Schematic representation shows the number of hypomethylated CpGs taking place in key cell subpopulations between NBC and P1.

(F) Characterization of hypomethylated CpGs into chromatin states between is shown. Blue, depletion; yellow, enrichment.

(G) Multiple genes associated with PC differentiation show hypomethylation in P1 and plasmablasts as compared to NBCs (same color scheme and methylation scale as in B).

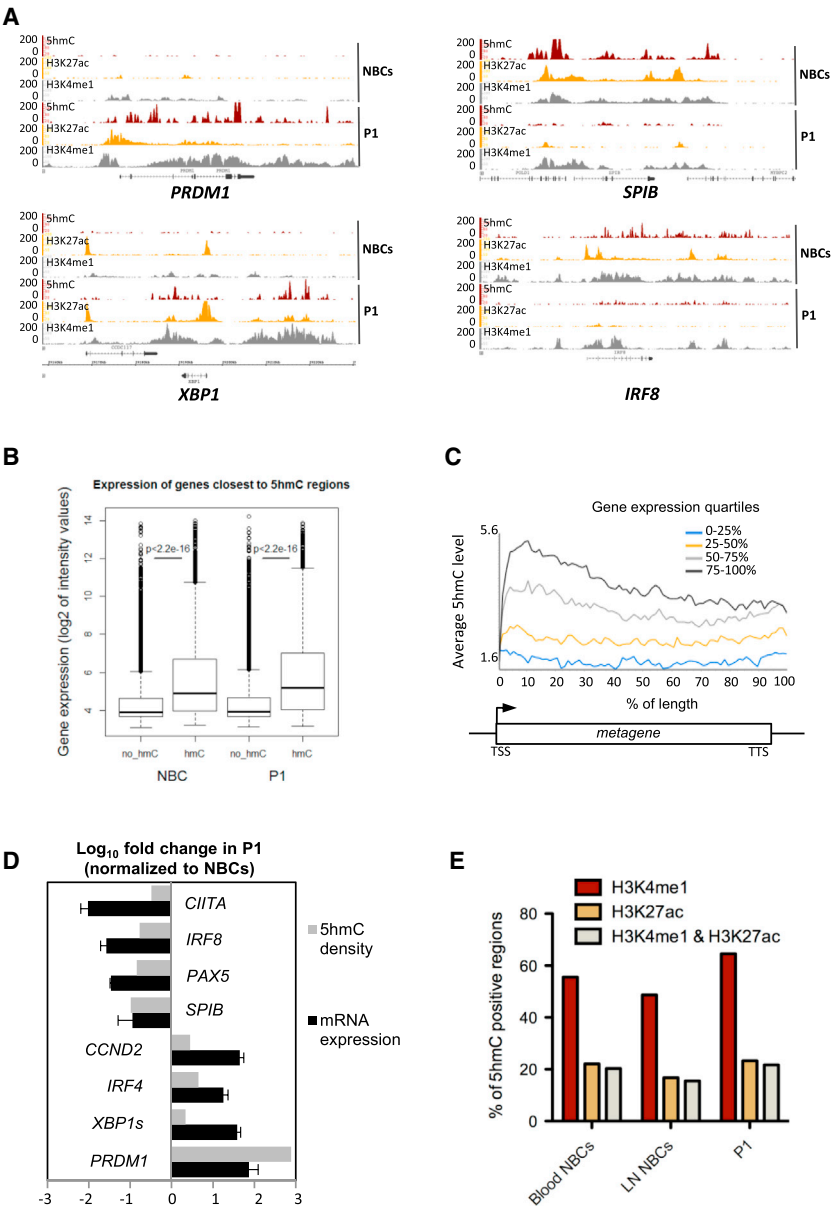

Figure 5. Genome-wide and Gene-Specific Analysis of 5hmC-Enriched Regions from NBCs and Plasmablasts

(A) Variations in intragenic 5hmC levels and histone modifications correlate with gene regulation during plasmablast differentiation. Integrated Genome Browser views show 5hmC, H3K4me1, and H3K27ac levels in genes activated (*PRDM1* and *XBP1*) or repressed (*SPIB* and *IRF8*) during differentiation for NBCs and P1.

(B) Genes that are associated with 5hmC-enriched regions have a significantly higher expression when compared to genes devoid of 5hmCs in NBCs and P1 cells ($p < 2.2e{-}16$, Wilcoxon rank-sum test).

(C) Metagene average profile of 5hmC enrichment according to P1 gene expression levels. Quartiles of genes were obtained based on transcriptomic data. Blue line, least expressed genes; black line, highest expressed genes.

(D) Relative mRNA expression (black bars; mean values ± SD; n = 3) and 5-hmC density (gray bars; reads densities in counts per million [cpm], background substracted, at gene loci ±100 kb) for selected genes in P1 cells compared to NBCs are shown.

(E) Overlap between 5hmC-enriched regions and H3K4me1- and H3K27ac-positive regions in NBCs and P1 cells. Bars indicate the percentage of 5hmC-positive regions that also are positive for either H3K4me1 (dark brown) or H3K27ac (orange) or both (gray).

differentiation of NBCs into P1 cells (Figure S5A, left). In addition, 5hmC levels were even lower in tonsil-derived plasmablasts and almost undetectable in human bone marrow-derived PCs from healthy donors (Figure S5A, right). This global loss in DNA hydroxymethylation could reflect a passive demethylation process due to a dilution of 5mC during multiple rounds of DNA synthesis or an absence of 5hmC maintenance during cell differentiation. Consistent with the latter hypothesis, TET expression levels decreased dramatically throughout the cell differentiation process (Figure S5B). However, 5hmC maps generated from blood and lymph node (LN) NBCs as well as from plasmablasts (P1 cells and purified plasmablasts) indicated that, although the number of identified hydroxymethylated unique regions decreased between LN NBCs (24,405; p = 1e−8) and P1 cells (12,542; p = 1e−8), specific regions gained 5hmC during differentiation (Figures 5A and S6A). Importantly, B cell identity genes lost 5hmC in P1, whereas PC identity genes gained 5hmC in P1 together with chromatin marks of active enhancers (H3K4me1 and H3K27ac, Figure 5A). Accordingly, a positive correlation between gene expression levels and DNA 5-hydroxymethylation was observed (Figure 5B) and was particularly prominent in gene bodies (Figure 5C). This correlation also was true for selected NBC- and plasmablast-expressed genes (Figure 5D), suggesting that changes in 5hmC levels mirror those in gene expression, a behavior that might apply to most down- and upregulated genes during plasmablast differentiation (Figure S6B).

At a global level, a dramatic redistribution of the 5hmC peaks was observed in P1 cells compared to LN NBCs as suggested by their poor overlap (12.4%, Figure S6C), although 5hmC was mainly enriched in introns and intergenic regions for both cell types (Figure S6D). A comparison of the genome-wide distribution of 5hmC with that of active enhancer marks (H3K4me1 and H3K27ac) indicated that, as already observed in other cell systems (Sérandour et al., 2012; Shen et al., 2013; Stroud et al., 2011), a large fraction of 5hmC-enriched regions might be related to enhancers (Figure 5E). These observations also are consistent with the fact that 25%–51% of hypomethylated CpGs during the differentiation process were located in

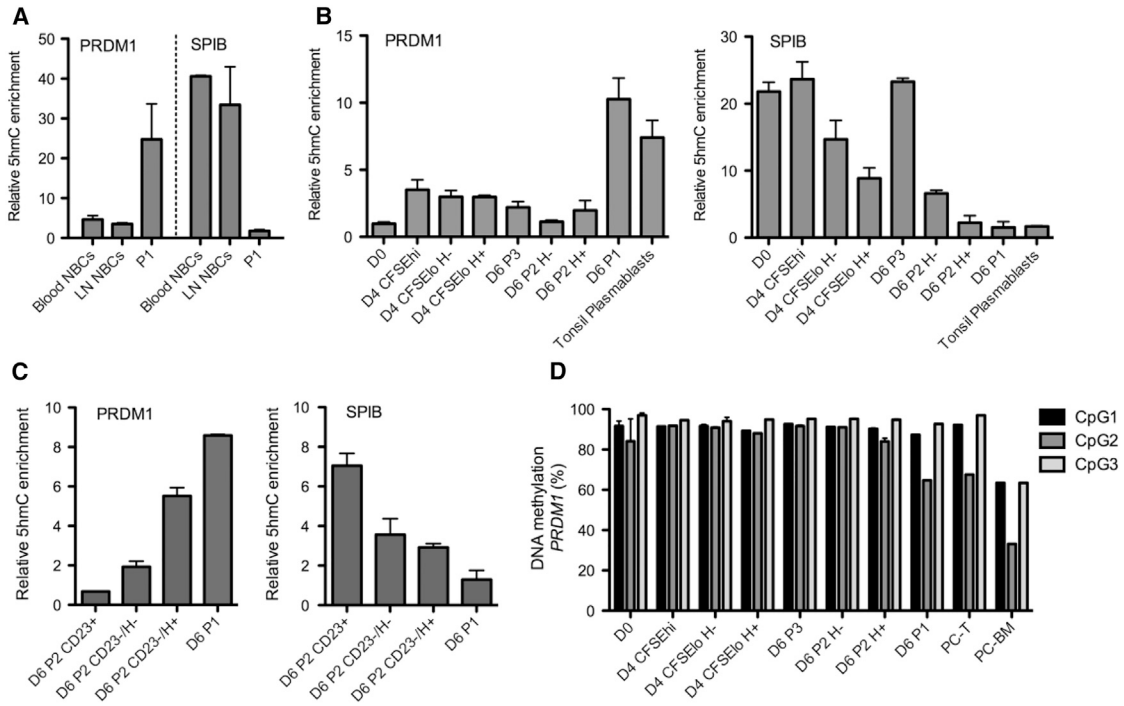

Figure 6. SCL-qPCR Analysis of 5hmC Enrichment in Genomic Regions of *PRDM1* and *SPIB*

(A–C) 5hmC enrichment at *PRDM1* (A–C, left) and *SPIB* (A–C, right) in the indicated cell-sorted compartments (n = 3). Note that *PRDM1*- and *SPIB*-associated hydroxymethylation could not be detected by SCL-qPCR in genomic DNA from bone marrow PCs.

(D) Pyrosequencing analysis of the methylation status of three CpGs included in the PRDM1 region analyzed by SCL-qPCR (n = 1–3 per CpG and cell subpopulation).

enhancers (Figure 4F), suggesting that these regulatory regions undergo active DNA demethylation. Collectively, these data indicate that changes in the transcriptome during NBC differentiation toward plasmablasts are accompanied by a dramatic reorganization of the pool of active enhancers, which are characterized by an active turnover of cytosine modifications.

The kinetics of cytosine hydroxymethylation events occurring at *SPIB* and *PRDM1* next were interrogated through SCL-qPCR (Figure 6A), and data revealed that changes in 5hmC levels correlated with the gene expression changes depicted in Figures 1E and 3E. Interestingly, *PRDM1* 5hmC levels started to rise only once P2 cells had lost the CD23 marker and underwent division (H+/P2 cells), indicating that targeting of *PRDM1* by TET activity is coupled with S/G2 phase progression (Figures 6B and 6C). Bisulfite conversion and pyrosequencing revealed that the DNA methylation levels of three CpGs included in the PRDM1 region analyzed by SCL-qPCR did not show clear significant variations between cell states except for bone marrow-derived PCs, which had a 30% reduction in DNA methylation (Figure 6D). This observation indicates that methylation of these particular CpGs was pre-established in NBCs and, hence, that *PRDM1* hydroxymethylation in CD23−/P2 cells may not require de novo methylation at these sites. Furthermore, the reduction in DNA methylation levels in PCs suggests that cytosine hydroxymethylation in *PRDM1* may represent an intermediate step of DNA demethylation in plasmablasts and P1 cells.

DISCUSSION

Our study characterizes molecular events taking place when a human activated B cell switches to a plasmablast, an antibody-secreting precursor of the long-lived PC. Our findings support a model that relies on two major processes: (1) a continuous integration of extracellular signals inducing cell proliferation and waves of DNA demethylation, notably at enhancers; and (2) a committal step where the cell cycle clock is precisely synchronized with and coordinates a plasmablastic differentiation switch, reflected by the selective occurrence of 5hmC in regions enriched in specific PC identity genes (Figure 7).

Consistent with a normal germinal center reaction, only highly proliferative cells can differentiate into PCs in an in vitro model of B cell differentiation (Tangye et al., 2003). B cell differentiation is sustained by an extensive reconfiguration of gene expression patterns and of the epigenetic landscape of the cell, including a progressive loss of DNA methylation (Kulis et al., 2015; Lai et al., 2013; Lee et al., 2012). In this study, a two-step differentiation protocol could transform human blood NBCs into a cell population (P1) that could not be distinguished from human tonsil-derived plasmablasts. This process depended on the emergence of plasmablast founder cells in the P2 population, characterized by their exit from the apoptotic program and their capacity to *re*cycle in the absence of BCR cross-linking, TLR activation, and CD40 stimulation. In the absence of IL-2 during the first step of cell culture, generation of plasmablasts was

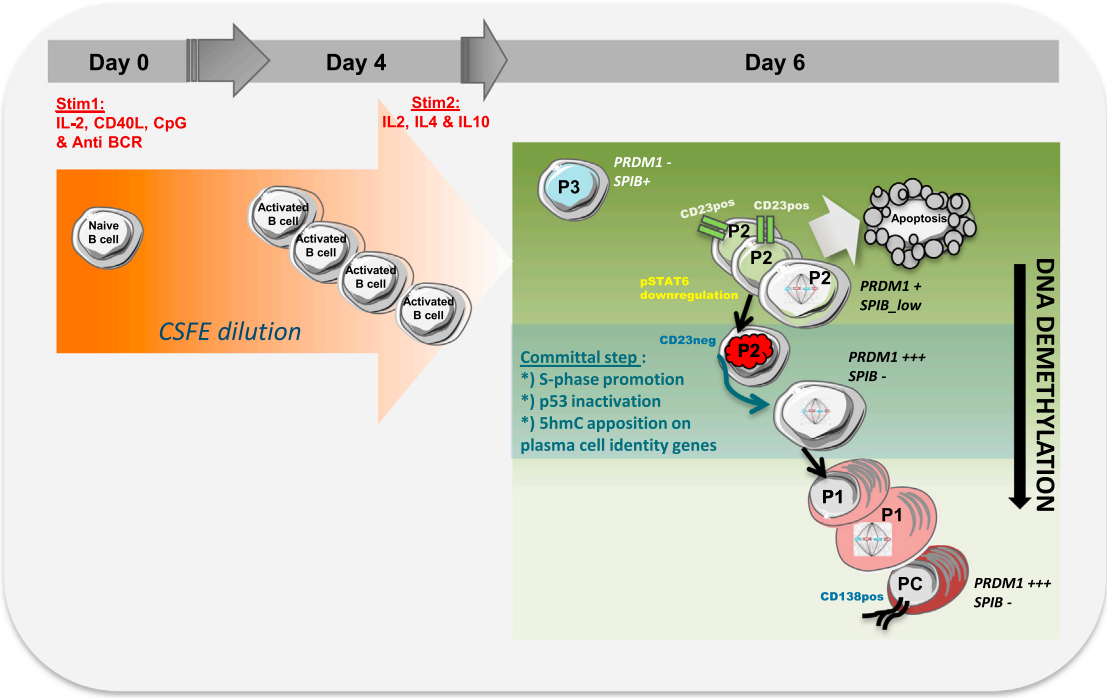

Figure 7. Schematic Representation of Human NBC Differentiation and Destiny

During the first 4 days (left), B cells proliferate and dilute the CFSE stain in response to the first stimulation cocktail (stim1) that induces IL-2, CD40, TLR, and BCR signaling. Between D4 and D6 (right), cells under influence of the second stimulation cocktail (stim2, including only cytokines) can acquire two alternative states as follows: lowly divided P3 cells and highly divided P2 cells. P2 cells upregulate *PRDM1*, downregulate *SPIB*, maintain cell divisions, and frequently undergo apoptosis. In addition, these cells are characterized by a proliferation-dependent DNA demethylation drift. A small fraction of P2 cells can emerge as CD23-negative/STAT-6-negative founder plasmablasts (red nucleus P2 cell) that undergo a committal step of B cell differentiation characterized by G1-S and S phase promotion, p53 pathway inhibition, and specific apposition of 5hmC on PC identity genes. This epigenetic phenomenon is likely to sustain high expression of PC fate-determining genes including *PRDM1*, allowing full maturation of PCs. PB, plasmablast.

impeded without affecting the capacity of P2 cells to proliferate (Le Gallou et al., 2012), suggesting that only cells that integrated a proper number of external cues were able to undergo final differentiation. Although commitment toward plasmablasts already was distinguishable after 4 days in culture (as assessed by *BCL6* and *BACH2* expression), cells underwent cell death beyond D4 unless they were able to trigger a molecular switch turning off the p53 pathway and IL4/STAT6 signaling. Subsequently, cells lost the membrane marker CD23, reflecting their transition from B cell identity to plasmablastic destiny. Our data suggest that this committal step takes place during the S phase of the cell cycle and requires S phase progression of cells undergoing a TGF-β1/SMAD3-regulated G1/S transition.

Since this final differentiation process seemed to be cell cycle dependent, we hypothesized that going through an S phase progression could provide a window for chromatin remodeling events required for transcriptional switches (Bird, 2002; Bird et al., 1998; Pop et al., 2010). Consistent with data obtained on sorted human mature B cells engaged in an immune response (Lai et al., 2013), we uncovered a high correlation among cell proliferation, levels of differentiation, and DNA demethylation. DNA demethylation occurred progressively with cell culture time and became particularly extensive at the final step of differentiation. A global evaluation of 5hmC levels in genomic DNA from various cell states showed a striking decrease during differentiation, with in-vitro-generated or primary plasmablasts maintaining very low 5hmC levels, whereas 5hmC was undetectable in long-lived PCs. Although these 5hmC levels were not high enough to be detected with ox-BS-450K arrays (data not shown), the use of the highly sensitive SCL procedure allowed us to evidence a selective gain in 5hmC during differentiation at genes and enhancers related to PC identity.

High levels of BLIMP1 are required to get fully mature PCs (Kallies et al., 2004), and the selective 5hmC enrichment of *PRDM1* during the last step of differentiation could participate in the setup of a chromatin state, allowing high transcription of this gene. Consistent with this hypothesis, we evidenced a general correlation between gene expression and 5hmC presence in gene bodies, suggesting that, despite the very low levels of 5hmC detected in P1 cells, 5hmC might be functionally relevant in these cells and impact on the establishment of a plasmablast-specific transcriptome. Here we have further explored this relationship by studying the kinetics of 5hmC apposition at *PRDM1* by SCL-qPCR in parallel to the analysis of the methylation status of three specific CpGs by pyrosequencing. Although stable DNA methylation was detected throughout the cell culture period, 5hmC apposition was found to occur specifically in CD23− and Hoechst+ cells of the P2 population. These later

also presented the closest gene expression profile compared to the one of plasmablasts, suggesting that targeting of *PRDM1* by TET activity is coupled with S phase progression and activation of the gene. Although a link between DNA synthesis and cytosine hydroxymethylation has not yet been evidenced, TET proteins could be targeted to replication forks through association with PCNA, as suggested from interaction assays in cancer cell lines (Cartron et al., 2013).

Hence, the molecular control of PC generation involves a precise committal step during which activated B cells escaping cell death turn on plasmablast fate-determining genes, most likely as a result of an active and cell cycle-synchronized demethylation process.

EXPERIMENTAL PROCEDURES

Primary B Cell Purification

Peripheral blood mononuclear cells (PBMCs) from healthy volunteers were obtained from the Etablissement Français du Sang after Ficoll density centrifugation (Sigma-Aldrich). NBCs were purified by negative selection using magnetic cell separation (Naive B Cell Isolation kit II, Miltenyi Biotech), following the manufacturer's instructions, using the AutoMACS deplete-sensitive program. Purity of isolated CD19+/CD27− NBCs was routinely above 99%. Reactive lymph node-derived NBCs, as well as tonsil plasmablasts, were isolated as previously described (Caron et al., 2009). CD38hi/CD138+ PCs were purified from bone marrow aspirates obtained from patients undergoing cardiac surgery. Subjects were recruited under institutional review board approval and informed consent according to the Declaration of Helsinki.

Cell Culture, Immunophenotyping, and Cell Sorting

Cell culture conditions, antibodies, and flow cytometry procedures were as previously described (Le Gallou et al., 2012). Briefly, purified human NBCs were labeled with 1 μM CFSE (Invitrogen) for 10 min before subsequent cell culture at 7.5 × 10^5 cells/ml in 24-well plates and stimulation with cocktail 1 described in Figure 1A for 4 days. Activated B cells were then washed and further cultured with cocktail 2 (Figure 1A).

After surface staining, the Cytofix/Cytoperm kit (BD Biosciences) was used for intracellular staining of active caspase-3 and IgG. Proliferation was analyzed using an antigen-presenting cell (APC)-conjugated anti-BrdU kit (BD Biosciences) according to the manufacturer's instructions.

For qRT-PCR analyses, B cells were isolated at D4, D5, or D6 by fluorescence-activated cell sorting (FACS) with an ARIA cell sorter (BD Biosciences) after DAPI (Sigma-Aldrich) staining to exclude dead cells. For cell sorting according to DNA content, cells were incubated at 2 × 10^6/ml in culture medium for 30 min at 37°C in the presence of 5 μg/ml Hoechst 33342 (Sigma-Aldrich).

qRT-PCR Analysis

RNA was extracted using RNeasy microkit (QIAGEN) and reverse transcribed into cDNA with Superscript II (Invitrogen). The qRT-PCRs were performed using the TaqMan Universal Master Mix and assays-on-demand from Applied Biosystems. Gene expression levels were quantified using *ABL1* as endogenous control. The 2 exp(−ΔΔCt) method was used to determine the relative expression of each gene. Data were compared using the Mann-Whitney test (GraphPad Prism Software).

Gene Expression Profiling

RNA samples of five cell populations (D4lo, D4hi, P1, P2, and P3) were hybridized onto Affymetrix Human Genome U219 Array Plates according to Affymetrix standard protocols. The analysis of scanned images for each probe set of the array was obtained with GeneChip Operating Software (GCOS, Affymetrix). Raw CEL files were processed and normalized with the robust multichip average (RMA) algorithm using R statistical software in conjunction with the Affy library available through Bioconductor. One-way repeated-measures ANOVA was used (false discovery rate [FDR] < 5%) to determine the genes that differed significantly between at least two of the five cell populations. Subsequent analyses were performed on these differentially expressed genes only.

Gene clusters were obtained from an unsupervised hierarchical clustering method using Euclidean distance and average linkage for clustering samples and Pearson's dissimilarity and Ward's method for clustering probe sets. By averaging the gene expressions within these clusters, we defined supergenes that were used to display a concise summary of the changes across time points and across cell populations. Paired two-tailed t test was used to identify the differentially expressed genes between two distinct populations as well as between each population versus all the other populations. In this last case, gene expressions of all other populations were averaged in the linear domain then log transformed for each subject prior to t test analysis. Canonical pathways and biological functions were generated by Ingenuity Pathways Analysis (Ingenuity Systems). These statistical analyses were performed using Partek Genomic Suite (version 6.6). Microarray data, as well methylation and hydroxymethylation data, are publicly available at GEO: GSE72498.

DNA Methylation Analysis Using 450K Microarray

We used the EZ DNA Methylation Kit (Zymo Research) for bisulfite conversion of 500 ng genomic DNA. Bisulfite-converted DNA was hybridized onto the HumanMethylation 450K BeadChip kit (Illumina), which covers 99% of RefSeq genes and 96% of CpG islands. The Infinium methylation assay was carried out following the manufacturer's instructions. Data from the 450K HumanMethylation array were analyzed in R using the minfi package (version 1.6.0) available through Bioconductor. For more details, see the Supplemental Experimental Procedures.

Bisulfite Pyrosequencing

The DNA methylation status of three CpGs of *PRDM1* was quantified in sorted cell subpopulations by bisulfite pyrosequencing using the PyroMark Q96 ID sequencer (QIAGEN), as previously described (Tost and Gut, 2007). DNA methylation levels were quantified with the PyroMark CpG software (QIAGEN). For primers details, see the Supplemental Experimental Procedures.

Genome-wide Mapping of 5hmC and Data Analysis

Genomic DNA (7 μg) from NBCs and plasmablasts was fragmented to 200–500 bp by sonication (Bioruptor, Diagenode) before incubation with β-glucosyltransferase and azide-glucose. Glucosylated 5hmCs were then labeled with biotin before enrichment of the biotinylated DNA fragments with streptavidin-coated magnetic beads. All steps used reagents from the Hydroxymethyl Collector kit (Active Motif). After elution from the beads, purified DNA was precipitated and processed for sequencing on a Highseq2000 (Illumina). Library preparations and sequencing reactions were run at the Institut de Génétique et de Biologie Moléculaire et Cellulaire (IGBMC) genomic platform. Unique sequencing reads were mapped to the reference genome (hg19) using bowtie (Langmead et al., 2009) allowing one mismatch. For more details on analysis and PCR primers for SCL-PCR, see the Supplemental Experimental Procedures. For correlation analysis of 5hmC enrichment and gene expression data, see the Supplemental Experimental Procedures.

ChIP-Seq Procedure

Chromatin immunoprecipitation sequencing (ChIP-seq) was performed in P1 cells following standard protocols generated within the Blueprint Consortium. Briefly, cells were fixed for 8 min in 1% formaldehyde at room temperature and chromatin was sonicated for 15 min with the Bioruptor Sonication System (Diagenode). Immunoprecipitation was carried out with antibodies from Diagenode against H3K4me1 (pAb-194-050, lot A1863-001P) and H3K27ac (pAb-196-050, lot A1723-0041D), using approximately 500,000 cells per antibody. ChIP-seq libraries were constructed using the Kapa Hyper Prep Kit (Kapa Biosystems). For each experiment, from 26 to 81 million reads were sequenced with an Illumina HiSeq1500 sequencer. Detailed protocols can be obtained from the Blueprint Consortium: http://www.blueprint-epigenome.eu/index.cfm?p=7BF8A4B6-F4FE-861A-2AD57A08D63D0B58.

ACCESSION NUMBERS

The accession number for the data reported in this paper is GEO: GSE72498.

SUPPLEMENTAL INFORMATION

Supplemental Information includes Supplemental Experimental Procedures, six figures, and one table and can be found with this article online at http://dx.doi.org/10.1016/j.celrep.2015.09.051.

AUTHOR CONTRIBUTIONS

G.C. performed the research, cell sorting, design of some experiments, and wrote the paper. M.H. performed the research, cell culture, and qPCR. M.K. performed methylation array analysis. C.D. performed gene expression microarray analysis and read the paper. F.C. participated in 5hmC, histone marks analysis, and correlation with expression data. A.P. did cell cultures and qPCR. S.A. did genome-wide sequencing analysis. M.L. performed TET expression investigation. E.A.M. performed SCL-qPCR. N.V.-D. prepared the ChIP-seq librairies. A.C.Q. did the pyrosequencing. K.T. helped in the design of the study. J.I.M.-S. designed, performed, and supervised methylation analysis. G.S. designed, performed, and supervised hydroxymethylation analysis and wrote the paper. T.F. designed the cell differentiation model, supervised the project, and wrote the paper.

ACKNOWLEDGMENTS

This work was supported by an internal grant from the Hematology laboratory, Pôle de biologie, CHU de Rennes, France; the Ligue Nationale contre le Cancer (Equipe labellisée); and the European Union's Seventh Framework Program through the Blueprint Consortium. M.H. was supported by a research grant from La Ligue contre le Cancer/Région Bretagne. G.S. was supported by the CNRS and the University of Rennes 1 and by grants from La Ligue contre le Cancer and Cancéropole Grand Ouest. E.A.M. was supported by a Ph.D. fellowship from the Ministère de l'enseignement supérieur et de la recherche. We are indebted to Delphine Rossille for her help on microarray analysis and Cédric Ménard for his help in providing mature bone marrow PCs. Sequencing was performed by the IGBMC Microarray and Sequencing platform, a member of the France Génomique consortium (ANR-10-INBS-0009), and the Biogenouest Genomics/Human & Environmental Genomics core facility of Rennes (Biosit/OSUR). Cell sorting was performed at the Biosit Flow Cytometry and Cell Sorting Facility (University of Rennes 1, France).

Received: November 17, 2014
Revised: July 6, 2015
Accepted: September 17, 2015
Published: October 22, 2015

REFERENCES

Allman, D.M., and Cancro, M.P. (2011). pERKing up the BLIMP in plasma cell differentiation. Sci. Signal. *4*, pe21.

Bird, A. (2002). DNA methylation patterns and epigenetic memory. Genes Dev. *16*, 6–21.

Bird, J.J., Brown, D.R., Mullen, A.C., Moskowitz, N.H., Mahowald, M.A., Sider, J.R., Gajewski, T.F., Wang, C.R., and Reiner, S.L. (1998). Helper T cell differentiation is controlled by the cell cycle. Immunity *9*, 229–237.

Caron, G., Le Gallou, S., Lamy, T., Tarte, K., and Fest, T. (2009). CXCR4 expression functionally discriminates centroblasts versus centrocytes within human germinal center B cells. J. Immunol. *182*, 7595–7602.

Cartron, P.F., Nadaradjane, A., Lepape, F., Lalier, L., Gardie, B., and Vallette, F.M. (2013). Identification of TET1 Partners That Control Its DNA-Demethylating Function. Genes Cancer *4*, 235–241.

Cattoretti, G., Shaknovich, R., Smith, P.M., Jäck, H.M., Murty, V.V., and Alobeid, B. (2006). Stages of germinal center transit are defined by B cell transcription factor coexpression and relative abundance. J. Immunol. *177*, 6930–6939.

Cedar, H., and Bergman, Y. (2011). Epigenetics of haematopoietic cell development. Nat. Rev. Immunol. *11*, 478–488.

Cubedo, E., Maurin, M., Jiang, X., Lossos, I.S., and Wright, K.L. (2011). PRDM1/Blimp1 downregulates expression of germinal center genes LMO2 and HGAL. FEBS J. *278*, 3065–3075.

Duffy, K.R., Wellard, C.J., Markham, J.F., Zhou, J.H., Holmberg, R., Hawkins, E.D., Hasbold, J., Dowling, M.R., and Hodgkin, P.D. (2012). Activation-induced B cell fates are selected by intracellular stochastic competition. Science *335*, 338–341.

Ernst, J., Kheradpour, P., Mikkelsen, T.S., Shoresh, N., Ward, L.D., Epstein, C.B., Zhang, X., Wang, L., Issner, R., Coyne, M., et al. (2011). Mapping and analysis of chromatin state dynamics in nine human cell types. Nature *473*, 43–49.

Huang, Y., Pastor, W.A., Shen, Y., Tahiliani, M., Liu, D.R., and Rao, A. (2010). The behaviour of 5-hydroxymethylcytosine in bisulfite sequencing. PLoS ONE *5*, e8888.

Jourdan, M., Caraux, A., Caron, G., Robert, N., Fiol, G., Rème, T., Bolloré, K., Vendrell, J.P., Le Gallou, S., Mourcin, F., et al. (2011). Characterization of a transitional preplasmablast population in the process of human B cell to plasma cell differentiation. J. Immunol. *187*, 3931–3941.

Kallies, A., Hasbold, J., Tarlinton, D.M., Dietrich, W., Corcoran, L.M., Hodgkin, P.D., and Nutt, S.L. (2004). Plasma cell ontogeny defined by quantitative changes in blimp-1 expression. J. Exp. Med. *200*, 967–977.

Kallies, A., Hasbold, J., Fairfax, K., Pridans, C., Emslie, D., McKenzie, B.S., Lew, A.M., Corcoran, L.M., Hodgkin, P.D., Tarlinton, D.M., and Nutt, S.L. (2007). Initiation of plasma-cell differentiation is independent of the transcription factor Blimp-1. Immunity *26*, 555–566.

Koh, K.P., Yabuuchi, A., Rao, S., Huang, Y., Cunniff, K., Nardone, J., Laiho, A., Tahiliani, M., Sommer, C.A., Mostoslavsky, G., et al. (2011). Tet1 and Tet2 regulate 5-hydroxymethylcytosine production and cell lineage specification in mouse embryonic stem cells. Cell Stem Cell *8*, 200–213.

Kriaucionis, S., and Heintz, N. (2009). The nuclear DNA base 5-hydroxymethylcytosine is present in Purkinje neurons and the brain. Science *324*, 929–930.

Kulis, M., Heath, S., Bibikova, M., Queirós, A.C., Navarro, A., Clot, G., Martínez-Trillos, A., Castellano, G., Brun-Heath, I., Pinyol, M., et al. (2012). Epigenomic analysis detects widespread gene-body DNA hypomethylation in chronic lymphocytic leukemia. Nat. Genet. *44*, 1236–1242.

Kulis, M., Merkel, A., Heath, S., Queirós, A.C., Schuyler, R.P., Castellano, G., Beekman, R., Raineri, E., Esteve, A., Clot, G., et al. (2015). Whole-genome fingerprint of the DNA methylome during human B cell differentiation. Nat. Genet. *47*, 746–756.

Kuo, T.C., Shaffer, A.L., Haddad, J., Jr., Choi, Y.S., Staudt, L.M., and Calame, K. (2007). Repression of BCL-6 is required for the formation of human memory B cells in vitro. J. Exp. Med. *204*, 819–830.

Lai, A.Y., Mav, D., Shah, R., Grimm, S.A., Phadke, D., Hatzi, K., Melnick, A., Geigerman, C., Sobol, S.E., Jaye, D.L., and Wade, P.A. (2013). DNA methylation profiling in human B cells reveals immune regulatory elements and epigenetic plasticity at Alu elements during B-cell activation. Genome Res. *23*, 2030–2041.

Langmead, B., Trapnell, C., Pop, M., and Salzberg, S.L. (2009). Ultrafast and memory-efficient alignment of short DNA sequences to the human genome. Genome Biol. *10*, R25.

Le Gallou, S., Caron, G., Delaloy, C., Rossille, D., Tarte, K., and Fest, T. (2012). IL-2 requirement for human plasma cell generation: coupling differentiation and proliferation by enhancing MAPK-ERK signaling. J. Immunol. *189*, 161–173.

Lee, S.T., Xiao, Y., Muench, M.O., Xiao, J., Fomin, M.E., Wiencke, J.K., Zheng, S., Dou, X., de Smith, A., Chokkalingam, A., et al. (2012). A global DNA methylation and gene expression analysis of early human B-cell development reveals a demethylation signature and transcription factor network. Nucleic Acids Res. *40*, 11339–11351.

Madzo, J., Liu, H., Rodriguez, A., Vasanthakumar, A., Sundaravel, S., Caces, D.B., Looney, T.J., Zhang, L., Lepore, J.B., Macrae, T., et al. (2014). Hydroxymethylation at gene regulatory regions directs stem/early progenitor cell commitment during erythropoiesis. Cell Rep. *6*, 231–244.

Martins, G., and Calame, K. (2008). Regulation and functions of Blimp-1 in T and B lymphocytes. Annu. Rev. Immunol. *26*, 133–169.

Mellén, M., Ayata, P., Dewell, S., Kriaucionis, S., and Heintz, N. (2012). MeCP2 binds to 5hmC enriched within active genes and accessible chromatin in the nervous system. Cell *151*, 1417–1430.

Nutt, S.L., Taubenheim, N., Hasbold, J., Corcoran, L.M., and Hodgkin, P.D. (2011). The genetic network controlling plasma cell differentiation. Semin. Immunol. *23*, 341–349.

Ochiai, K., Maienschein-Cline, M., Simonetti, G., Chen, J., Rosenthal, R., Brink, R., Chong, A.S., Klein, U., Dinner, A.R., Singh, H., and Sciammas, R. (2013). Transcriptional regulation of germinal center B and plasma cell fates by dynamical control of IRF4. Immunity *38*, 918–929.

Pastor, W.A., Pape, U.J., Huang, Y., Henderson, H.R., Lister, R., Ko, M., McLoughlin, E.M., Brudno, Y., Mahapatra, S., Kapranov, P., et al. (2011). Genome-wide mapping of 5-hydroxymethylcytosine in embryonic stem cells. Nature *473*, 394–397.

Pop, R., Shearstone, J.R., Shen, Q., Liu, Y., Hallstrom, K., Koulnis, M., Gribnau, J., and Socolovsky, M. (2010). A key commitment step in erythropoiesis is synchronized with the cell cycle clock through mutual inhibition between PU.1 and S-phase progression. PLoS Biol. *8*, e1000484.

Ray, D., Terao, Y., Nimbalkar, D., Chu, L.H., Donzelli, M., Tsutsui, T., Zou, X., Ghosh, A.K., Varga, J., Draetta, G.F., and Kiyokawa, H. (2005). Transforming growth factor beta facilitates beta-TrCP-mediated degradation of Cdc25A in a Smad3-dependent manner. Mol. Cell. Biol. *25*, 3338–3347.

Sérandour, A.A., Avner, S., Oger, F., Bizot, M., Percevault, F., Lucchetti-Miganeh, C., Palierne, G., Gheeraert, C., Barloy-Hubler, F., Péron, C.L., et al. (2012). Dynamic hydroxymethylation of deoxyribonucleic acid marks differentiation-associated enhancers. Nucleic Acids Res. *40*, 8255–8265.

Shen, L., Wu, H., Diep, D., Yamaguchi, S., D'Alessio, A.C., Fung, H.L., Zhang, K., and Zhang, Y. (2013). Genome-wide analysis reveals TET- and TDG-dependent 5-methylcytosine oxidation dynamics. Cell *153*, 692–706.

Song, C.X., Szulwach, K.E., Fu, Y., Dai, Q., Yi, C., Li, X., Li, Y., Chen, C.H., Zhang, W., Jian, X., et al. (2011). Selective chemical labeling reveals the genome-wide distribution of 5-hydroxymethylcytosine. Nat. Biotechnol. *29*, 68–72.

Stroud, H., Feng, S., Morey Kinney, S., Pradhan, S., and Jacobsen, S.E. (2011). 5-Hydroxymethylcytosine is associated with enhancers and gene bodies in human embryonic stem cells. Genome Biol. *12*, R54.

Szulwach, K.E., Li, X., Li, Y., Song, C.X., Wu, H., Dai, Q., Irier, H., Upadhyay, A.K., Gearing, M., Levey, A.I., et al. (2011). 5-hmC-mediated epigenetic dynamics during postnatal neurodevelopment and aging. Nat. Neurosci. *14*, 1607–1616.

Tahiliani, M., Koh, K.P., Shen, Y., Pastor, W.A., Bandukwala, H., Brudno, Y., Agarwal, S., Iyer, L.M., Liu, D.R., Aravind, L., and Rao, A. (2009). Conversion of 5-methylcytosine to 5-hydroxymethylcytosine in mammalian DNA by MLL partner TET1. Science *324*, 930–935.

Tangye, S.G., Avery, D.T., and Hodgkin, P.D. (2003). A division-linked mechanism for the rapid generation of Ig-secreting cells from human memory B cells. J. Immunol. *170*, 261–269.

Tost, J., and Gut, I.G. (2007). DNA methylation analysis by pyrosequencing. Nat. Protoc. *2*, 2265–2275.

Yin, Y., Tainsky, M.A., Bischoff, F.Z., Strong, L.C., and Wahl, G.M. (1992). Wild-type p53 restores cell cycle control and inhibits gene amplification in cells with mutant p53 alleles. Cell *70*, 937–948.

Zhang, H.S., Gavin, M., Dahiya, A., Postigo, A.A., Ma, D., Luo, R.X., Harbour, J.W., and Dean, D.C. (2000). Exit from G1 and S phase of the cell cycle is regulated by repressor complexes containing HDAC-Rb-hSWI/SNF and Rb-hSWI/SNF. Cell *101*, 79–89.